Inorganic Chemistry
Article
pubs.acs.org/IC

Design of Medium Band Gap Ag–Bi–Nb–O and Ag–Bi–Ta–O Semiconductors for Driving Direct Water Splitting with Visible Light

Limin Wang,[†,¶] Bingfei Cao,[†] Wei Kang,[‡,#] Mark Hybertsen,[‡] Kazuhiko Maeda,[§,∥,○] Kazunari Domen,[§] and Peter G. Khalifah*[,†,⊥]

[†]Department of Chemistry, Brookhaven National Laboratory, Upton, New York 11973-5000, United States

[‡]Center for Functional Nanomaterials, Brookhaven National Laboratory, Upton, New York 11973-5000, United States

[§]Department of Chemical System Engineering, University of Tokyo, 7-3-1 Hongo, Bunkyo-ku, Tokyo 113-8656, Japan

[∥]Precursory Research for Embryonic Science and Technology (PRESTO), Japan Science and Technology Agency (JST), 4-1-8 Honcho Kawaguchi, Saitama 332-0012, Japan

[⊥]Department of Chemistry, Stony Brook University, Stony Brook, New York 11794-3400, United States

Supporting Information

ABSTRACT: Two new metal oxide semiconductors belonging to the Ag–Bi–*M*–O (*M* = Nb, Ta) chemical systems have been synthesized as candidate compounds for driving overall water splitting with visible light on the basis of cosubstitution of Ag and Bi on the *A*-site position of known $Ca_2M_2O_7$ pyrochlores. The low-valence band edge energies of typical oxide semiconductors prevents direct water splitting in compounds with band gaps below 3.0 eV, a limitation which these compounds are designed to overcome through the incorporation of low-lying Ag $4d^{10}$ and Bi $6s^2$ states into compounds of nominal composition "$AgBiM_2O_7$". It was found that the "$AgBiTa_2O_7$" pyrochlores are in fact a solid solution with an approximate range of $Ag_xBi_{5/6}Ta_2O_{6.25+x/2}$ with $0.5 < x < 1$. The structure of $Ag_{4/5}Bi_{5/6}Ta_2O_{6.65}$ was determined from the refinement of time-of-flight neutron diffraction data and was found to be a cubic pyrochlore with a = 10.52268(2) Å and a volume of 1165.143(6) Å^3. The closely related compound, $AgBiNb_2O_7$, appears to have an integer stoichiometry and to adopt an orthorhombically distorted pyrochlore-related structure with a subcell of a = 7.50102(8) Å, b = 7.44739(7) Å, c = 10.5788(1) Å, and V = 590.93(2) Å^3. Density functional theory-based calculations predict this distortion should result from *A*-site cation ordering. Fits to UV–vis diffuse reflectance data suggest that $AgBiNb_2O_7$ and "$AgBiTa_2O_7$" are both visible-light-absorbing semiconductors with the onset of strong direct absorption at 2.72 and 2.96 eV, respectively. Electronic structure calculations for an ordered $AgBiNb_2O_7$ structure show that the band gap reduction and the elevation of the valence band primarily result from hybridized Ag d^{10}–O 2p orbitals that lie at higher energy than the normal O 2p states in typical pyrochlore oxides. While the minimum energy gap is direct in the band structure, the lowest energy dipole allowed optical transitions start about 0.2 eV higher in energy than the minimum energy transition and involve different bands. This suggests that the minimum electronic band gap in these materials is slightly smaller than the onset energy for strong absorption in the optical measurements. The elevated valence band energies of the niobate and tantalate compounds are experimentally confirmed by the ability of these compounds to reduce 2 H^+ to H_2 gas when illuminated after functionalization with a Pt cocatalyst.

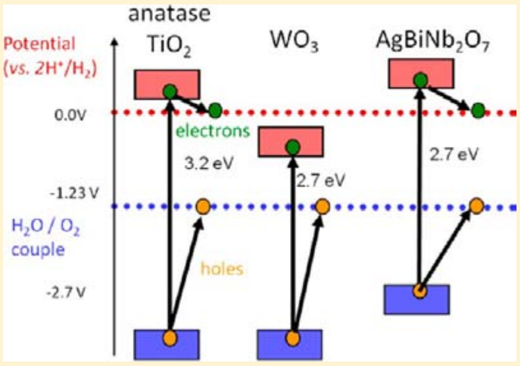

■ INTRODUCTION

The discovery of new visible-light-responsive semiconductors for water splitting is an important step toward meeting the challenge of efficiently and economically producing renewable H_2 fuel using solar energy. The use of sunlight to split water for H_2 fuel is a very promising strategy for the renewable production of H_2 through the reaction $2\ H_2O + \text{light} \rightarrow 2\ H_2 + O_2$. The sun provides sufficient energy to earth to meet our societal demands if this reaction can be carried out with a good overall efficiency. To date, most materials capable of using light to split water can only do so by utilizing ultraviolet (UV) radiation.[1,2] Only a very small fraction of solar energy (~5%) consists of high energy UV photons, placing a severe upper bound on the overall efficiency of this process. Only a handful of materials[1,2] have been discovered to effectively split water using visible (vis) light photons (1.5–3.2 eV), and thus far, no stable material exhibits a visible light quantum efficiency larger than about 5% with the record held by the $(Ga_{1-x}Zn_x)(N_{1-x}O_x)$ solid solution system.[3] Although oxide materials have been studied for water splitting applications for more than 30 years, this field has experienced a recent renaissance driven by the application of novel synthetic, theoretical, and characterization methods to this historic problem, as detailed in some

Received: January 26, 2013
Published: July 31, 2013

recent reviews of the complex oxide materials under current consideration.[2,4,5]

Our pressing scientific challenge is to better understand the chemical and structural factors which influence the conduction band energy (CBE) and valence band energy (VBE) positions with the specific goal of raising the VBE to allow direct water splitting with visible light. While the CBE position varies strongly with elemental substitution in oxide semiconductors, the VBE is generally insensitive to such substitutions since it is typically composed almost entirely of oxygen 2p states. This situation implies that smaller band gap semiconductors, which provide an enhanced solar spectrum response, will not be thermodynamically able to reduce water to H_2. On the other hand, the standard oxide VBE position is far below what is necessary to drive the water splitting reaction, and produces a tremendous limitation to the overall efficiency of the photoelectrolytic water splitting process and the large-scale viability of this process. We therefore seek to discover materials whose VBE has a different chemical origin, and to guide our understanding of the factors influencing the VBE position.

Herein, two new materials, "$AgBiNb_2O_7$" and "$AgBiTa_2O_7$", have been synthesized on the basis of our strategy to alter the character of the VBE states by utilizing $d^{10}s^2$–d^0 configurations to push up the valence band levels while leaving the CBE largely invariant. These substitutions are designed to narrow the band gap in these semiconductors while still preserving their suitability for driving both half reactions of overall water splitting. The preparation and structural characterization of these new semiconductors, their optical properties, their electronic structures and the feasibility of these materials for visible-light-driven H_2 production will be discussed.

■ EXPERIMENTAL SECTION

Polycrystalline samples of "$AgBiNb_2O_7$" and "$AgBiTa_2O_7$" were synthesized by solid-state reaction. Powders of Ag_2O (Alfa, 99.99%), Bi_2O_3 (Alfa, 99.99%), and Nb_2O_5 or Ta_2O_5 (Alfa, 99.99%) were mixed and ground under acetone in an agate mortar and pestle. After drying, the powder was collected and put into a dense alumina crucible and covered with a lid. For "$AgBiNb_2O_7$", the molar ratio used to synthesize a single-phase product was $Ag_2O/Bi_2O_3/Nb_2O_5$ = 0.5:0.5:1, while for "$AgBiTa_2O_7$", the ratio was $Ag_2O/Bi_2O_3/Ta_2O_5$ = 0.4:0.418:1. Approximately 2 g of starting materials were heated in air at 600 °C for 15 h, ground, and then heated at 1000 °C for 24 h. Bright-yellow powders and pale-yellow powders were obtained with essentially unchanged compositions, which are denoted as $AgBiNb_2O_7$ and $Ag_{4/5}Bi_{5/6}Ta_2O_{6.65}$, respectively.

X-ray diffraction data for Rietveld refinement were collected at room temperature using a Bruker D8 Advance diffractometer equipped with a Cu K_α source (λ = 1.5418 Å), a Ni K_β filter (0.5 mm), an 0.6° divergence slit, and a radius of 300 mm. Data collection was done over a 2θ range of 5−120°, a 2θ step size of 0.01°, and a total integration time of 792 s per point when summed over the 192 channels of the LynxEye Si strip detector. Neutron diffraction data were collected on the POWGEN3 time-of-flight (TOF) diffractometer at the Spallation Neutron Source (SNS) at Oak Ridge National Lab during run cycle 2011-A. The powder sample (~2 g) was placed in a cylindrical vanadium can. Crystal structures were refined by the Rietveld method using TOPAS v4.2 (Bruker AXS), although similar results were also obtained using the GSAS/EXPGUI software packages in preliminary refinements.[6,7] Empirical absorption corrections were applied to the neutron data in TOPAS by scaling the data as d^{4-x} rather than the d^4 appropriate for TOF neutron diffraction data, where x was refined to 0.43 for the low d-spacing data with the vast majority of peaks collected in POWGEN "Frame 1.5" and to 0.57 for the high d-spacing data collected in POWGEN "Frame 4" which only had seven peaks. The conversion of time-of-flight to d-spacing was accomplished through the equation: TOF = $t_0 + t_1 \cdot d + t_2 \cdot d^2 + t_3 \cdot d^n$ where the power n in the nonstandard fourth term was allowed to refine to a value between four and five, enabling the peak positions to be effectively modeled over the expansive width of each frame. Only slight variations relative to the three parameters determined from an instrumental standard were observed. Indexing and Le Bail fits of "$AgBiNb_2O_7$" diffraction data to obtain lattice parameters were also done using the TOPAS v4.2 software package (Bruker AXS) using the X-ray diffraction data.

Density functional theory (DFT)-based calculations were utilized to study the known pyrochlore compound $Ca_2Nb_2O_7$ and a model cation-ordered "$AgBiNb_2O_7$" structure. The magnitude and nature of band gaps in these pyrochlore semiconductors were investigated, as were the magntitude of their optical response and the energy proximity of the onset of strong absorption relative to the band gap energy. The CASTEP program[8] as implemented in the Materials Studio package supplied by Accelrys was utilized with ultrasoft pseudopotentials[9] The cutoff energies for plane wave basis sets were 300−340 eV. The generalized gradient approximation (GGA) of Perdew, Bruker, and Ernzerhof (PBE)[10] was used for the exchange-correlation functional. The valence electron configurations were $3s^23p^64s^2$ for Ca, $4s^24p^64d^45s^1$ for Nb, $2s^22p^4$ for O, $4d^{10}5s^1$ for Ag, and $6s^26p^3$ for Bi. Geometry optimization was performed on the compounds starting from a cubic pyrochlore structure (8 formula units per unit cell) with a 2 × 2 × 2 Monkhorst−Pack grid to sample the Brillouin zone, and using the BFGS algorithm to obtain lattice parameters and atomic positions corresponding to the ground state (lowest energy) configurations. A Gaussian smearing of 0.1 eV was included in the density of states (DOS) and absorption plots. All of the DOS plots were shifted so that the Fermi level is placed at 0 eV.

For powder samples, UV−vis (ultraviolet−visible) diffuse reflectance spectra were collected on a PerkinElmer Lambda 950 spectrophotometer at room temperature from 200 to 1000 nm with powders of the large band gap semiconductor Al_2O_3 (Alfa, 99.99%) used as a reference blank. The collected reflectance data were transformed using the Kubelka−Munk function to obtain a response proportional to the absorption using the function: $\alpha_{KM} = (1-R)^2/2R = \alpha/s$, where α_{KM} is the relative absorbance obtained through this transform, R is the reflectance, α is the true (absolute) absorption coefficient, and s is the sample-specific scattering coefficient.

Photocatalytic reactions were performed using an inner-irradiation type vessel connected with a closed gas circulation system whose design has been previously described.[11] The reaction solution was evacuated prior to irradiation with a high-pressure Hg lamp (450 W) that was put in a water filter made of Pyrex glass to allow for $\lambda > 300$ nm sample irradiation. The spectral data for the lamp are provided in the Supporting Information (SI). The temperature of the reaction solution was maintained at room temperature by flowing cooling water through the outer jacket of the vessel. Evolved gases were quantified using a gas chromatograph equipped with a thermal conductivity detector that utilized Ar as carrier gas. In the H_2 production test, 0.3 g of sample were dispersed in 400 mL of methanol solution (H_2O/methanol = 9:1 by volume) with 0.1 wt % Pt cocatalyst loaded using *in situ* photodeposition (H_2PtCl_6 precursor, 97% Pt, Kanto Chemicals, Japan). For O_2 production testing, 0.2 g of sample were dispersed in 100 mL of 0.01 M $AgNO_3$ solution without any cocatalyst.

■ RESULTS AND DISCUSSION

While there have been many prior screening studies of oxide semiconductors that tested their activity for driving water-splitting reactions, our goal is to rationally design materials suitable for this purpose. Good semiconductors for light harvesting should be able to move photogenerated carriers from their interior to their surface. It is therefore desirable to focus on semiconductors with a three-dimensional network of M−O (metal−oxygen) bonds since these systems have the highest probability of having good charge carrier mobilities. The pyrochlore structure is one of the most common crystal structure types for oxides, and pyrochlore compounds have previously been reported to have activity for overall water splitting when illuminated with ultraviolet light.[1] Pyrochlore compounds typically have a formula of $A_2B_2X_7$, where the large A cation typically only plays a structural role while the smaller B cation is usually strongly bonded to and hybridized with the X anions in the material, which together form a conduction network through which electrons and holes move. We have chosen to explore pyrochlore compounds where the B cation is either Nb^{5+} or Ta^{5+}, due to the many prior reports of semiconducting behavior and water splitting activity in compounds with these d^0 cations.

Some canonical pyrochlore compounds include the wide band gap semiconductors $Ca_2Ta_2O_7$ (E_g = 4.40 eV[12]) and $Ca_2Nb_2O_7$ (E_g = 4.15 eV[13]), although it should be noted that these phases are only thermodynamically stable at relatively low temperatures and that their high-temperature polytypes have a different perovskite-related layered structure.[14] The large band gaps of these compounds make them clearly unsuitable for visible-light-driven water splitting (E_g < 3.0 eV is typically needed to absorb visible light photons with E_{ph} < 3.2 eV since the band gap only tracks the onset of absorption), an issue that we have worked to resolve by making chemical substitutions on the A-site of these pyrochlore compounds. Two strategies were followed for raising the valence band edge energy and reducing the band gap of these materials (Figure 1), potentially enabling direct water splitting with visible light. First, incorporating Bi^{3+} ions into the structure introduces low-lying Bi 6s states which are expected to repulsively interact with the O 2p valence band states that occur at somewhat higher energies. Second, adding Ag^+ ions into the structure will create a manifold of filled Ag $4d^{10}$ states, which can occur at higher energies than that of the O 2p states and which can supplant the oxygen states as the top of the valence band. We therefore targeted chemical compounds where the two Ca^{2+} atoms are replaced with one Ag^{1+} and one Bi^{3+} cation, giving rise to the target compositions of $AgBiTa_2O_7$ and $AgBiNb_2O_7$.

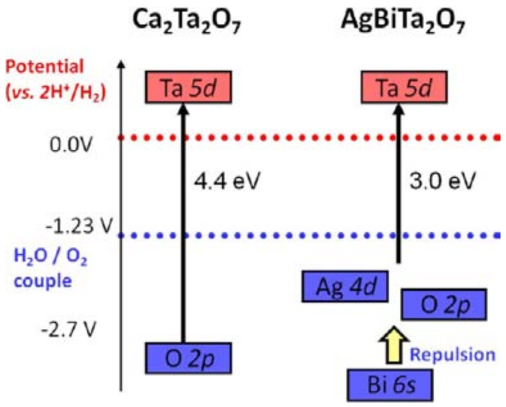

Figure 1. Schematic comparison of the known pyrochlore compound $Ca_2Ta_2O_7$ and the putative pyrochlore compound "$AgBiTa_2O_7$" emphasizing their different band gaps and the estimated positions of different atomic orbitals expected to dominate the conduction band (red) and valence band states (blue). The two factors designed to raise the valence band edge energy in "$AgBiTa_2O_7$" are repulsive interactions from low-lying Bi 6s states and filled Ag 4d states which may be higher in energy than the O 2p states that make up the valence band of typical oxide semiconductors.

Binary oxide precursors were mixed in this ratio and reacted at temperatures of 1000 °C, and the resulting powder diffraction patterns of the products had a series of peaks that at first glance appeared to be be belong to cubic pyrochlore materials with nominal formulas of "$AgBiTa_2O_7$" and "$AgBiNb_2O_7$". While we were able to synthesize stoichiometric "$AgBiNb_2O_7$", there were clear indications that true formulas of the stable compound differs from its nominal formula—we will use the notation "$AgBiTa_2O_7$" to refer to the single-phase quaternary tantalate compound that forms at our synthesis temperature in air with the knowledge that its actual composition deviates from $AgBiTa_2O_7$. The diffraction patterns of these single-phase materials are given in Figure 2. The compound "$AgBiTa_2O_7$" could be clearly and accurately be indexed with a cubic cell of a = 10.52 Å that corresponds to a pyrochlore structure. However, the single-phase tantalate product was only obtained from starting materials with a 1:1:2 ratio of Ag:Bi:Ta after a prolonged heating which resulted in a significant loss of the relatively volatile Ag and/or Bi species (as judged from measured mass changes during the synthesis reaction), indicating a marked deviation from the nominal cation stoichiometry. Further refinement of the synthetic procedure showed that a single-phase pyrochlore with the composition $Ag_{4/5}Bi_{5/6}Ta_2O_{6.65}$ could be made from starting materials with this stoichiometric ratio. Although the powder pattern of the "$AgBiNb_2O_7$" niobate product closely resembles that of the tantalate in peak positions and intensities, a very close inspection of the pattern indicates that the major diffraction peaks are split and that the symmetry of the phase is lower than cubic. However, the crystal structure is almost certainly pyrochlore-related, given the close similarity of the niobate and tantalate phase X-ray diffraction patterns. No known matches to the "$AgBiNb_2O_7$" structure could be found in searches of the 2010 JCPDS powder diffraction database.

Structure and Composition of "$AgBiTa_2O_7$". Given the close relationship of "$AgBiTa_2O_7$" to known pyrochlore structures, Rietveld refinement of powder diffraction data is suitable as a method for refining the crystal structure and stoichiometry of this phase. However, X-ray powder diffraction data alone is not sufficient for obtaining good structural information about this compound due to its insensitivity to the oxygen atoms which are a crucial part of the framework but which can have complex displacements and site vacancy patterns within the pyrochlore framework. In particular, the crystallography of Bi-containing pyrochlore oxides is often quite complex due to the presence of potentially cooperative displacements of A-site Bi^{3+} cations and O2-site oxygen anions away from their ideal positions, a result which has been well-established in powder, single-crystal, and theoretical studies,[15−19] making the collection of high-quality and high-resolution diffraction data particularly important. Therefore, time-of-flight neutron diffraction data were collected on the POWGEN beamline of the ORNL SNS facility, providing many well-resolved Bragg peaks out to a minimum d-spacing of about 0.3 Å. The Rietveld refinement of the "$AgBiTa_2O_7$" structure is shown in Figure 3, with the detailed crystallographic information presented in Tables 1 and 2.

An ideal model of the pyrochlore structure of "$AgBiTa_2O_7$" lacking displacive disorder was first tested, which gave the geometry shown on the left side of Figure 3. The ideal pyrochlore structure ($Fd\bar{3}m$, No. 227) is a three-dimensional network formed by corner-shared octahedra [BO_6] with A cations and O2-site oxygen anions filling hexagonal channels in

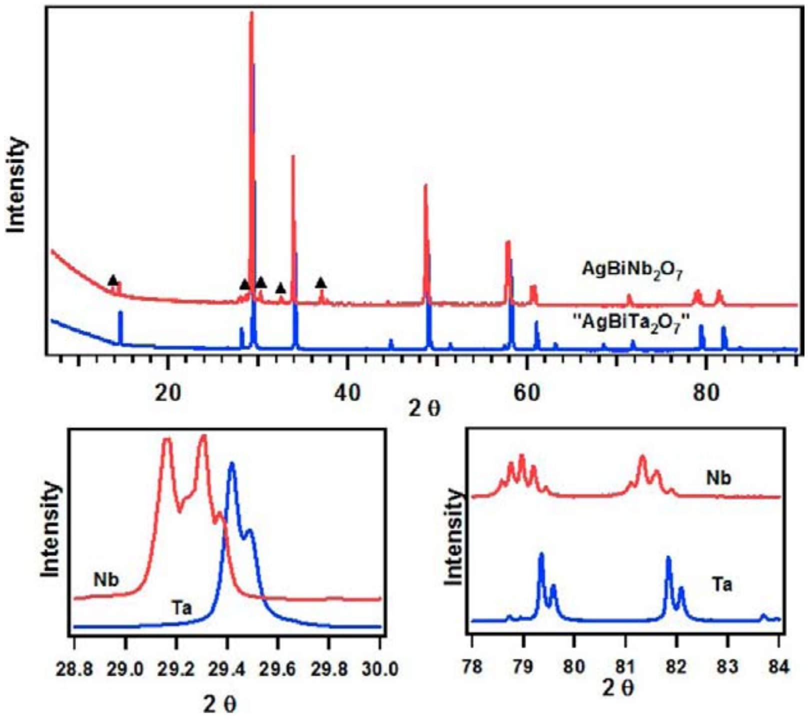

Figure 2. (Top) X-ray diffraction patterns of $AgBiNb_2O_7$ (red) and "$AgBiTa_2O_7$" (blue). The triangles indicate the peaks that cannot be indexed in a cubic structure. (Bottom) The enlargements show peak splitting of the $AgBiNb_2O_7$ phase around 30° (left) and 80° (right), respectively, indicating a structure distortion from cubic to lower symmetry.

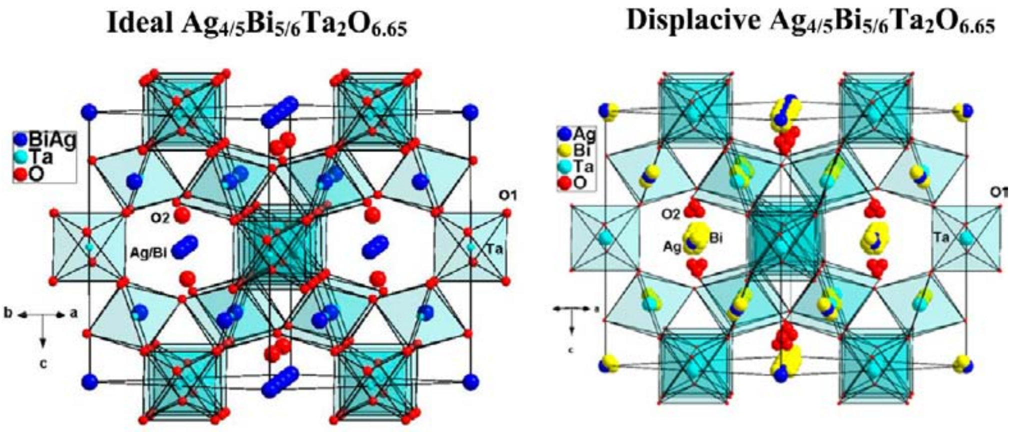

Figure 3. Crystal structure of $Ag_{4/5}Bi_{5/6}Ta_2O_{6.65}$ viewed along [110] direction with Ag and Bi atoms mixed on *A*-sites: ideal structure (left) and *A*-site and O′-site displacively disordered structure (right).

Table 1. $Ag_{4/5}Bi_{5/6}Ta_2O_{6.65}$ Rietveld Refinement Results

nominal stoichiometry	$Ag_{0.8}Bi_{0.836}Ta_2O_{6.654}$
refined formula	$Ag_{4/5}Bi_{5/6}Ta_2O_{6.65}$
space group	$Fd\bar{3}m$ (No. 227)
a (Å)	10.52268(2)
cell volume (Å^3)	1165.143(6)
Z	8
data resolution (*d*)	neutron: 0.33−3.3 Å
R values (%), standard structure	R_p = 2.960; R_{wp} = 2.268
R values (%), displacive structure	R_p = 2.978; R_{wp} = 2.269

the network. There are two different cation sites and two different anion sites in the pyrochlore structure with cation *A*-sites occupied with large cations (usually alkaline-earth and rare-earth metals) and cation *B*-sites occupied with small cations (usually transition metals). The atomic site information (labels, multiplicities/Wyckoff positions, and fractional atomic coordinates) with $Fd\bar{3}m$ origin choice 2 is: *A* - 16c (0, 0, 0), *B* - 16d (0.5, 0.5, 0.5), O1 - 48f (*x*, 0.125, 0.125), O2 - 8a (0.125, 0.125, 0.125). Since the O2-site anions are only bonded to *A* cations, the pyrochlore structure can be described as interpenetrating A_2O and B_2O_6 networks made up of three-dimensional corner-shared [OA_4] tetrahedra and [BO_6] octahedra, respectively. In the initial refinement within this ideal pyrochlore structure, the Ag/Bi and O2 atoms were placed in their usual special positions of 16c (0, 0, 0) and 8a (0.125, 0.125, 0.125), respectively. The B_{iso} of Ag/Bi and O2 atoms were found to be abnormally large (substantially exceeding those of the Ta and O atoms) in this model, potentially indicating deviations of those atoms from their ideal pyrochlore sites. A more complex displacive structural model

Table 2. Crystallographic Sites for Standard Model of $Ag_{4/5}Bi_{5/6}Ta_2O_{6.65}$

atom	Wyk	x	y	z	occ.	B_{iso} or B_{ij}
Ag	16c	0	0	0	0.40	$B_{11} = B_{22} = B_{33} = 3.1(4)$; $B_{12} = B_{13} = B_{23} = -0.94(11)$
Bi	16c	0	0	0	0.417	3.07(23)
Ta	16d	1/2	1/2	1/2	1	0.620(8)
O1	48f	0.43654(4)	1/8	1/8	1	$B_{11} = 1.007(15)$; $B_{22} = B_{33} = 1.152(11)$; $B_{12} = B_{13} = 0$; $B_{23} = -1.1(3)$
O2	8a	0.125	0.125	0.125	0.65	3.06(4)

Table 3. Crystallographic Sites for Displacive Model of $Ag_{4/5}Bi_{5/6}Ta_2O_{6.65}$

atom	Wyk	x	y	z	occ.	B_{iso} or B_{ij}
Ag	16c	0	0	0	0.25	$B_{11} = B_{22} = B_{33} = 2.35(14)$; $B_{12} = B_{13} = B_{23} = 0.73(8)$
Bi	96h	0	0.0186(5)	−0.0186(5)	0.0694	1.17(7)
Ta	16d	1/2	1/2	1/2	1	0.600(8)
O1	48f	0.43654(4)	1/8	1/8	1	$B_{11} = 0.972(15)$; $B_{22} = B_{33} = 1.154(11)$; $B_{12} = B_{13} = 0$; $B_{23} = -1.1(3)$
O2	32e	0.1372(3)	0.1372(3)	0.1372(3)	0.137	1.44(9)

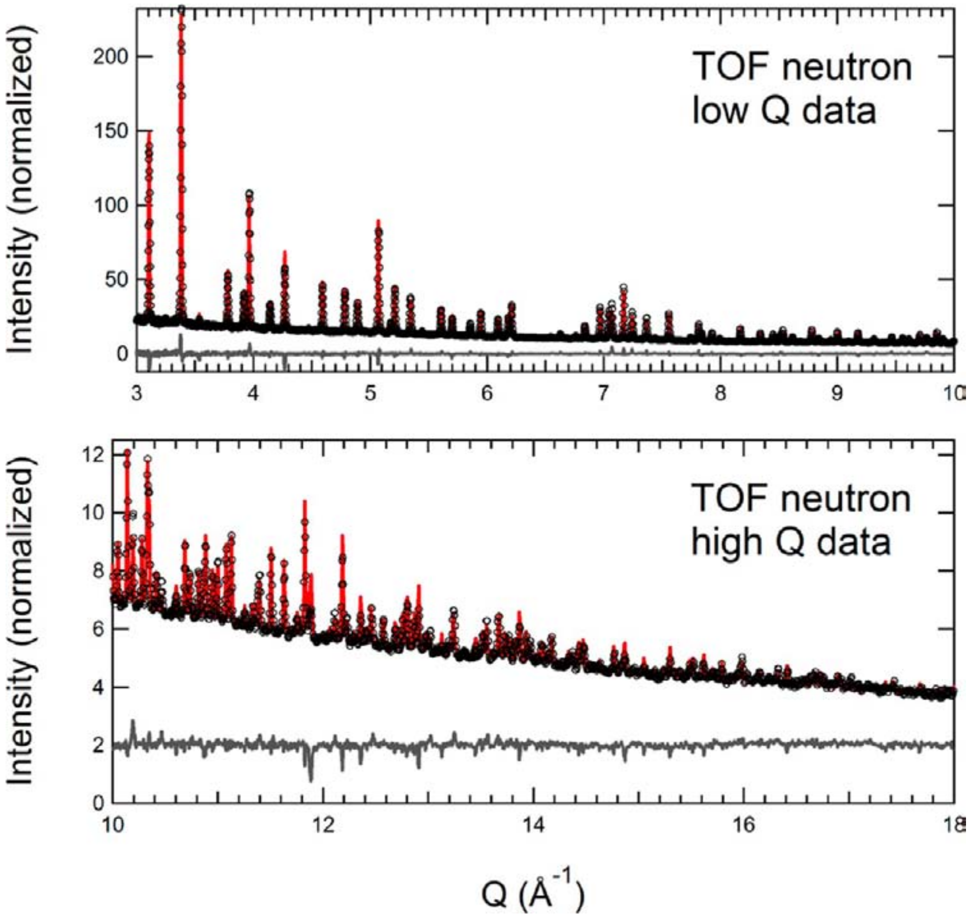

Figure 4. Calculated Rietveld refinement diffraction patterns for $Ag_{4/5}Bi_{5/6}Ta_2O_{6.65}$ in a displacive model (red lines) for POWGEN neutron diffraction data, with difference patterns shown in gray with appropriate offsets. Q (Å^{-1}) = $2\pi/d$ (Å).

was therefore used to describe the atomic positions of "$AgBiTa_2O_7$", generating a much more reasonable set of displacement parameters and bond lengths in the final structural refinement. These two models are presented and compared in Tables 1−3, and are discussed further below.

It is not unusual for pyrochlore compounds containing Bi on the *A*-site to exhibit displacive disorder since the asymmetry introduced by Bi lone pair electrons can prevent Bi atoms from sitting at the center of the ideal 6 + 2 coordination environment of the pyrochlore *A*-site.[16−19] The presence of the active Bi lone pairs on the *A*-site typically results in the O2 atoms also moving to a nonideal off-centered coordination environment that exhibits displacive disorder. The normal method of describing the displacive disorder of Bi-containing pyrochlores is to change the Bi atoms from fully occupying their 16c (0,0,0) ideal position and instead model them with an occupancy of 1/6 on the higher multiplicity 96g (*x*,*x*,*z*) or 96h (0,*y*,−*y*) sites (positions are described for origin choice 2 of the $Fd\bar{3}m$ space group). It has been previously reported the 96g and 96h sites are indistinguishable from powder diffraction refinement, though local structure studies of the Bi coordination environment in $(Bi,Zn)_2(Zn,Nb)_2O_7$ by extended X-ray absorption fine structure (EXAFS) found that the 96h site is preferred.[15−19] It should be noted that other displacement vectors are possible within the $Fd\bar{3}m$ space group, including (x,x,x) for the 32e site and the arbitrary (x,y,z) displacement of the general position (192i). The situation is more complicated in "$AgBiTa_2O_7$", since two different cations with unknown occupancies and with two different sizes (ionic radii of Ag^{1+} = 1.28 Å, Bi^{3+} = 1.17 Å for a coordination number of eight) are present on the pyrochlore *A*-site, one or both which may move off-center, and with cation vacancies of these volatile elements potentially also present on the *A*-site.

Given the need to refine both the position, occupancy, and isotropic displacement parameters of the Ag and Bi cations on the *A*-site (6−10 variables, depending on the model being tested), it is virtually impossible to freely refine all of these parameters since they all influence how the electron density is distributed over a common spatial region and will therefore refine in a strongly correlated manner. When models were constrained so that (1) the same displacive model was used for Ag and Bi and (2) the separation between the Ag and Bi positions was equal to their approximate size difference, it was consistently found that the refined displacements of Ag from the ideal position were significantly smaller than the magnitude of the vibrations implied by examining the square root of the isotropic displacement parameter of this cation. This suggested that the Ag cations should be left on the ideal pyrochlore *A*-site position. Searches within the 2011 version of Pearson's Crystal Database for previous structure determinations on pyrochlore compounds with *A*-site Ag cations found no prior examples of displaced Ag cations, though there were a very limited number of relevant reports.

The suitability of placing Ag on the ideal position was also evaluated through the calculation of the Ag bond valence sum (BVS) for different Ag coordinates on and off the ideal position, using the parametrization suggested by Brese and O'Keefe.[20] The BVS method assigns a fractional valence to each bonded anion coordinating a central cation assuming an exponential decay in valence with increasing bond length. Cation bond valence sum values (the sum of the individual bond valences of all coordinated anions) which are near the ideal cation valence indicate optimal bonding, while lower and higher valences demonstrate underbonding and overbonding, respectively, indicating that cations are at less favorable environments which are expected to be higher in free energy. The BVS values in valence units (vu) calculated for the ideal Ag position using both the ideal pyrochlore and Bi-displacive structural models are 1.20 vu and 1.22 vu, respectively. The calculated Ag valences are in reasonable agreement with the ideal valence of +1, and displacing Ag away from the ideal position results in an even larger degree of overbonding which should be thermodynamically disfavored. This is in marked contrast to the Bi site. The BVS value of Bi atoms situated in the ideal pyrochlore position is 2.37 vu, a value that improves to 2.52 when Bi is displaced off-site to the optimal position found by Rietveld refinement in the optimal $(0,y,-y)$ direction of the best displacive model (96h site position). For comparison, the refined Ta−O distance of 1.98 Å leads to a BVS value of 5.14 vu, and is a very normal environment for TaO_6 octahedra containing Ta^{5+}.

There is therefore both good literature precedent as well as theoretical and experimental justification for using a displacive model for Bi and O2 atoms but not for the Ag atoms, and the final neutron Rietveld refinement of this "$AgBiTa_2O_7$" structure (Figure 4) was done in this manner. The best results were obtained with the displaced Bi atoms at the 6-fold split 96h site (which corresponds to a displacement toward a pair of oxygen atoms in the hexagonal ring surrounding the *A*-site cations) while the Ag atoms were kept at the ideal 16c site and the O2 atoms were moved to the nonideal displacive 32e site resulting in 2-fold splitting of the atomic site. The structural effects of these displacements are visualized in Figure 5, while the resulting bond distances are given in Table 4.

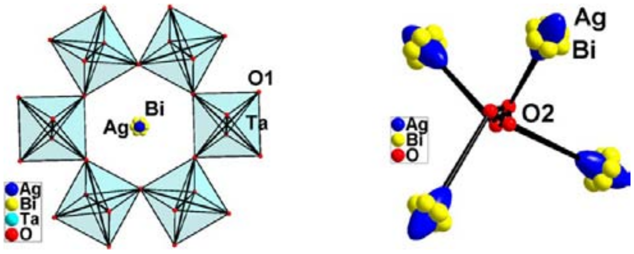

Figure 5. Coordination environment of *A* cations (left) and O2 anions (right) in displacively disordered pyrochlore structure, with 25% ellipsoids drawn.

Table 4. Comparison of Bond Distances (Å) for $Ag_{4/5}Bi_{5/6}Ta_2O_{6.65}$ Refined Using Standard and Displacive Pyrochlore Models

Standard Structure			
Ag−O1	2.7043(3) × 6	Bi−O1	2.7043(3) × 6
Ag−O2	2.27823 × 2	Bi−O2	2.27823 × 2
Ta−O1	1.9764(1) × 6		
Displacive Structure			
Ag−O1	2.7043(3) × 6	Bi−O1	2.471(6) × 2
Ag−O2	2.214(1) × 6 (75%)		2.718(1) × 2
	2.500(6) × 2 (25%)		2.946(6) × 2
Ta−O1	1.9764(3) × 6	Bi−O2	2.209(2) × 2 (25%)
			2.232(2) × 2 (25%)
			2.254(2) × 2 (25%)
			2.515(6) × 2 (25%)

Anisotropic displacement parameters were tested for each site with the constraint that they remain positive definite. A large improvement in the fit was obtained when the Ag site and O1 sites were modeled with anisotropic displacement parameters, but the influence on other sites was small, and isotropic displacement parameters were therefore used for all other sites in the final refinement. The O1 displacement ellipsoids were very flat in a mildly aphysical manner, with their thin axis nearly normal to the Ta−O bond lengths and pointing toward the *A*-site cations. The improvement in the refinement associated with using anisotropic displacement parameters for O1 atoms could also be replicated by splitting the O1 site in two, utilizing the 96g Wyckoff position with coordinates of (0.4365, 0.1177, 0.1323). This split site preserved the average Ta−O bond length of 1.98 Å, suggesting that the TaO_6 octahedra may undergo a cooperative rotation to optimize bonding with *A*-site cations. However, a full investigation of the nature of this rotation is beyond the scope of this paper, and the O1 ions were therefore refined on their ideal position with a large anisotropic displacement in the final refinement. The Ag anisotropic ellipsoids were found to have significant elongation along the cubic [111]-type directions (in accord with their site symmetry restriction of $B_{11} = B_{22} = B_{33}$ and $B_{12} = B_{23} = B_{31}$), with the ellipsoid major axis in this direction about three times longer than in the perpendicular directions (which lie in the plane of Bi displacements). This could be due to either atomic vibrations or atomic displacements to a two-fold split site in this direction as these two models are indistinguishable in the quality of their fit. The final refinement was carried out using Ag sites which were not split, in accordance with the predictions of BVS theory and in preference to the simpler nature of this model.

The occupancy of the Ta and O1 sites were set to be fully occupied, while the occupancy of the Ag and Bi cations (which could be more readily volatilized or lost to secondary amorphous or nanoscale phases) were allowed to refine to values less than the starting composition of the sample (Ag/Bi/Ta molar ratio of 0.8:0.836:2) with the one constraint that charge balance must be maintained through variation of the occupancy on the O2 site. Refinements consistently converged to produce maximal occupancy at the both the Ag and Bi sites, consistent with the negligible mass changes during synthesis and the absence of secondary phases in the diffraction pattern. In the final refinement the Bi occupancy was rounded to 5/6 while the Ag occupancy was set at 0.8, and both occupancies were fixed at these values. The O2 content was therefore fixed by charge balance to be 0.65 per formula unit. This number was in reasonable agreement with the value obtained when the O2 content was freely refined (~0.75), though it should be noted that the site splitting does impair the ability of Bragg diffraction techniques to probe the site occupancy since the form factor from this relatively diffuse site drops off more quickly with increasing Miller index than for localized sites. A close inspection of the nuclear density in the vicinity of the O2 site reconstructed from a Fourier difference map showed circumstantial evidence for excess nuclear density that was nearly spherical in shape which might correspond to a third (O3) oxygen site at a position of (0.0785, 0.0785, 0.0785) midway between the ideal O2 position and the ideal *A*-site position. This site could account for about one-quarter of the oxygen content not associated with the O1 site, though the improvement of the refinement when this O2 site was utilized was small. As a result, this site was not utilized in the final refinement. Future neutron diffraction studies on closely related compositions will be carried out to obtain a better understanding of the significance of this potential O3 site in the context of the bonding preferences of Ag and Bi.

The idealized stoichiometry of $Ag_{4/5}Bi_{5/6}Ta_2O_{6.65}$ was therefore chosen to describe "$AgBiTa_2O_7$" in the final refinement (Figure 4), on the basis of its proximity to the nominal stoichiometry and on the basis of its crystal chemical relationship to the pyrochlore structure. Only small peaks in the difference pattern were observed over the entire breadth of the fitting range (~0.33−3.3 Å). The values of displacement parameters are often a good metric for judging physical correctness, and they are quite reasonable in magnitude for the final refined structure of $Ag_{4/5}Bi_{5/6}Ta_2O_{6.65}$. This pyrochlore phase is clearly deficient in *A*-cations (Ag, Bi) relative to the simple integer stoichiometry of "$AgBiTa_2O_7$" which was originally postulated. When synthesized, the nominal stoichiometry of "$AgBiTa_2O_7$" equilibrates to a three-phase mixture of pyrochlore, $BiTaO_4$, and Ag metal phases, confirming that the integer stoichiometry of "$AgBiTa_2O_7$" does not correctly describe the pyrochlore phase. While many other pyrochlores with A-site vacancies are known, it is still worth considering the origin of the atypical stoichiometry of this compound.

In the closely related silver antimonate pyrochlore $Ag_2Sb_2O_6$ where Ag fully occupies the pyrochlore *A*-site, the O2-site is completely vacant in a manner which facilitates the bonding preferences associated with the low valence of Ag^+. An examination of the ~30 pyrochlore compounds in Pearson's Crystal database that contain Ag^+ on the pyrochlore *A*-site shows no examples of structures where the O2-site is fully occupied by O^{2-} anions, suggesting that vacancies on the O2-site are required for Ag−Bi−Ta−O pyrochlores. X-ray diffraction studies on samples with related compositions with variable silver contents suggests that $Ag_{4/5}Bi_{5/6}Ta_2O_{6.65}$ is located in the middle of a broader $Ag_xBi_{5/6}Ta_2O_{6.25+x/2}$ solid solution with approximate solubility limits of $0.5 \leq x \leq 1.0$ whose lattice parameters very weakly depend on the Ag content, and which span a range of oxygen contents from 6.5 to 6.75 per formula unit. The perpendicular direction in phase space has not been explored to the same level of detail, but it was observed that Bi-rich stoichiometries (e.g., $Ag_{0.7}BiTa_2O_z$) could produce a two-phase mixture with $BiTaO_4$ while Bi-poor stoichiometries (e.g., $Ag_{0.886}Bi_{0.67}Ta_2O_z$) could produce a two-phase mixture with $AgTaO_3$, establishing the two-phase regions which bound the solid solution. There is as yet no evidence for a nonzero width of solid solution with regard to the Bi content, and if a range of Bi contents can be supported, this width must be substantially narrower than for Ag. There are numerous examples of Bi-containing pyrochlores with fully occupied *A*-sites, so the low fraction of Bi in the present system is curious. The very different Ag^+ and Bi^{3+} site preferences and bonding preferences (Ag^+ requires partial or full vacancies on neighboring O2 sites, while Bi^{3+} is underbonded even when O2 sites are fully occupied) are anticipated to interact in a complex manner that is perhaps further mediated by cooperative tilts of TaO_6 octahedra inferred from the large O1 displacement parameters. Further structural investigations across the full range of $Ag_xBi_{5/6}Ta_2O_{6.25+x/2}$ pyrochlore using a combination of bulk and local probes will be required to fully understand the chemical interactions that lead to the complex observed stoichiometries

Structure and Composition of "$AgBiNb_2O_7$". Syntheses based on starting materials with the stoichiometric ratio of "$AgBiNb_2O_7$" successfully produced a single phase with no significant impurity peaks that could not be indexed against structural databases and therefore likely represents both a previously unknown phase and a previously unknown structure. In addition to preparing a sample with the nominal composition of "$AgBiNb_2O_7$", a set of additional samples were made whose starting molar ratios varied by 10−20% and were also reacted at the same temperature to probe the Ag−Bi−Nb−O phase diagram at 1000 °C, the compositions of which are marked in Figure 6. All of the trial off-stoichiometric compositions resulted in a smaller fraction of the new phase and more substantial quantities of previously known impurity phases ($BiNbO_4$, Nb_2O_5, $AgNbO_3$, Ag_2O, or $Bi_5AgNb_4O_{18}$) in X-ray diffraction patterns. When the starting stoichiometry of "$AgBiNb_2O_7$" was used, the mass loss during the heat treatment was small (< 0.2 %), indicating that the true stoichiometry should indeed be the nominal stoichiometry of $AgBiNb_2O_7$.

A coarse examination of the X-ray diffraction patterns of $AgBiNb_2O_7$ and $Ag_{4/5}Bi_{5/6}Ta_2O_{6.65}$ suggests that they have very similar structures, as judged by the similar positions and intensities of the major peaks (Figure 4, top), though the fact that the peaks of $AgBiNb_2O_7$ are split clearly indicates a lower symmetry lattice for this phase with small deviations from the

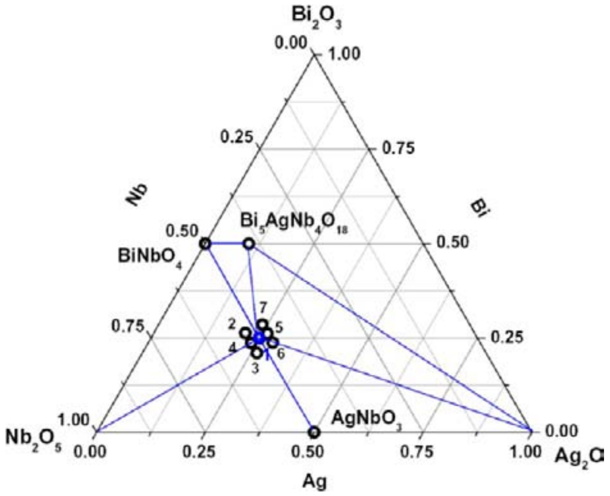

Figure 6. Ternary phase diagram of $Ag_2O-Bi_2O_3-Nb_2O_5$ system with trial compositions of: 1 - $AgBiNb_2O_7$, 2 - $Ag_{0.8}BiNb_2O_7$, 3 - $AgBi_{0.8}Nb_2O_7$, 4 - $Ag_{0.9}Bi_{0.9}Nb_2O_7$, 5 - $Ag_{1.1}Bi_{1.1}Nb_2O_7$, 6 - $Ag_{1.2}BiNb_2O_7$, 7 - $AgBi_{1.2}Nb_2O_7$.

ideal cubic atomic arrangement of $Ag_{4/5}Bi_{5/6}Ta_2O_{6.65}$. One possible origin for the symmetry distortion is the presence of *A*-site cation ordering between Ag and Bi atoms, perhaps driven by the substantially different coordination preferences of these ions observed in $Ag_{4/5}Bi_{5/6}Ta_2O_{6.65}$. This hypothesis was tested by generating an ordered arrangement of Ag and Bi atoms at the ideal *A*-site positions within a cubic cell and then using density functional theory (DFT) to relax the structure to an energy minimum (Figure 7). The symmetry of this relaxed structure was analyzed and found to be orthorhombic in the *Imma* (No. 74) space group, with lattice parameters of a = 7.6333 Å, b = 7.4466 Å, and c = 10.6764 Å. The crystallographic relationships between the original cubic pyrochlore cell and the orthorhombic cell are apparent through the square root of two reduction in the *a*- and *b*-axes lengths together with an unmodified *c*-axis length. It should also be noted that the reduced cell volume is essentially unchanged (~300 Å^3) between the two different lattices with different centering operations. From this theoretical starting point, it was possible to fit the experimentally observed split positions of the major peaks of "$AgBiNb_2O_7$" to a unit cell of a = 7.50102(8) Å, b = 7.44739(7) Å, c = 10.5788(1) Å, and V = 590.93(2) Å^3. All three cell axes represent deviations of less that 0.4% from the corresponding cubic ideal, resulting in a high degree of overlap between X-ray diffraction peaks.

It should be noted that the true space group and lattice of $AgBiNb_2O_7$ must be different from the orthorhombic *Imma* lattice that was used to successfully index all of the most intense peaks of this phase in a Le Bail fit, since a few weak peaks remained unindexed (marked with crosses in the top panel of Figure 8). X-ray diffraction pattern analysis for the off-

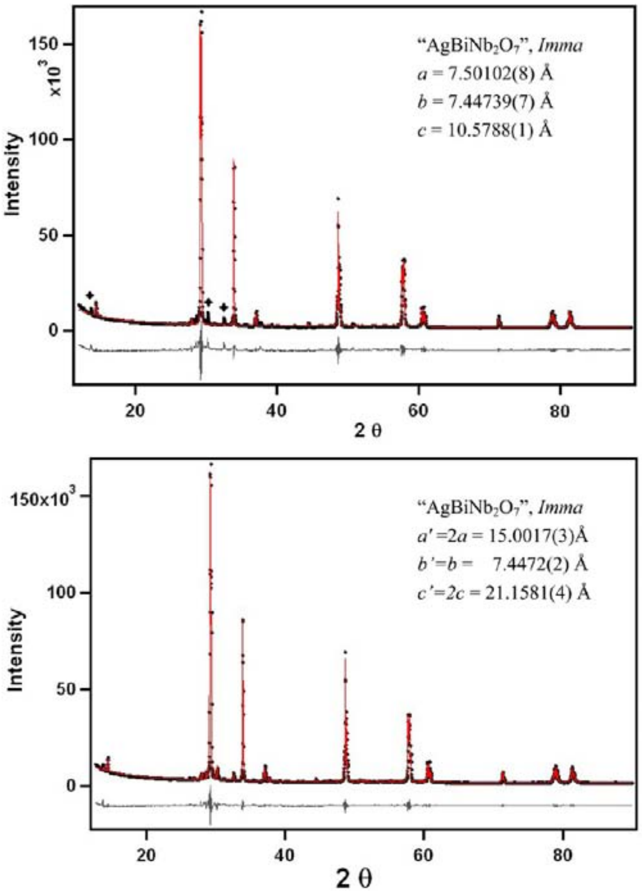

Figure 8. Le Bail fitting of "$AgBiNb_2O_7$" in space group *Imma*, with (top) a = 7.50102(8) Å, b = 7.44739(7) Å, c = 10.5788(1) Å and (bottom) a = 15.0017(3) Å, b = 7.4472(2) Å, c = 21.1581(4) Å. Crosses indicate unindexed peaks associated with this phase.

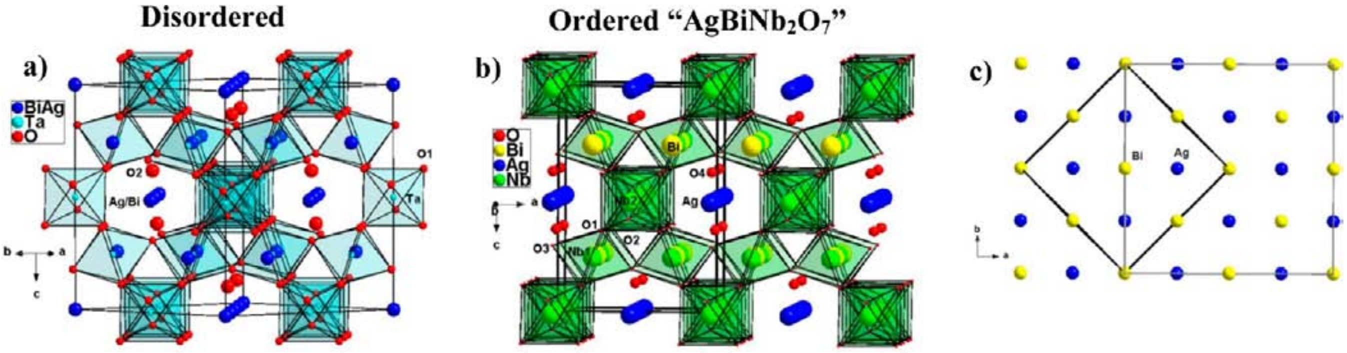

Figure 7. Crystal structure of (a) $Ag_{4/5}Bi_{5/6}Ta_2O_{6.65}$ viewed along the [110] direction with Ag, Bi atoms disordered over the pyrochlore *A*-site with displacements omitted for clarity and (b) hypothetical "$AgBiNb_2O_7$" structure viewed along [010] direction with an ordered arrangement of Ag and Bi atoms on the *A*-site. (c) Sketch showing the relationship of a typical cubic pyrochlore cell and the orthorhombic cell derived for *A*-site ordered "$AgBiNb_2O_7$".

stoichiometric samples prepared to investigate the phase diagram showed that the intensities of these weak unindexed peaks scaled with those of the known "$AgBiNb_2O_7$" peaks, and therefore did not originate with sample impurities. Furthermore, these weak peaks could be indexed using a Le Bail fit to a quadruple-volume supercell of the *Imma* cell (doubled *a*- and *c*-axes) as illustrated in the bottom panel of Figure 8. This indicates that "$AgBiNb_2O_7$" may have either a supercell featuring small displacements of atoms away from their ideal subcell positions or a commensurate modulation of its atoms, the latter being judged more likely as it would more readily explain why so few peaks require an additional lattice periodicity to be indexed. Once the structure of this distorted pyrochlore phase is solved, it is anticipated that valuable insights will be gained into the bonding preferences of Ag and Bi ions mixed within a pyrochlore framework and the influence of these bonding preferences on the unusual observed stoichiometry of Ag−Bi−Ta-O pyrochlores.

Electronic Structures and Optical Properties. The compounds $AgBiNb_2O_7$ and $Ag_{4/5}Bi_{5/6}Ta_2O_{6.65}$ were synthesized with the goal of realizing oxide semiconductors with raised valence band levels and reduced band gaps which can efficiently utilize visible light to drive photochemical reactions. It is therefore very important to understand the influence of the changed electronic states of $AgBiNb_2O_7$ and $Ag_{4/5}Bi_{5/6}Ta_2O_{6.65}$ (relative to $Ca_2Nb_2O_7$ and $Ca_2Ta_2O_7$) on their absorption spectra. Figure 9 shows the measured absorption spectra of these compounds obtained from a Kubelka−Munk analysis of room temperature diffuse reflectance data. Both compounds show sharp absorption transitions below 3.0 eV, indicating that they are rare examples of niobates and tantalates capable of absorbing visible light across their semiconductor band gap. This can be directly seen in the pale-yellow color of $Ag_{4/5}Bi_{5/6}Ta_2O_{6.65}$ powders and in the intense yellow color of $AgBiNb_2O_7$ powders.

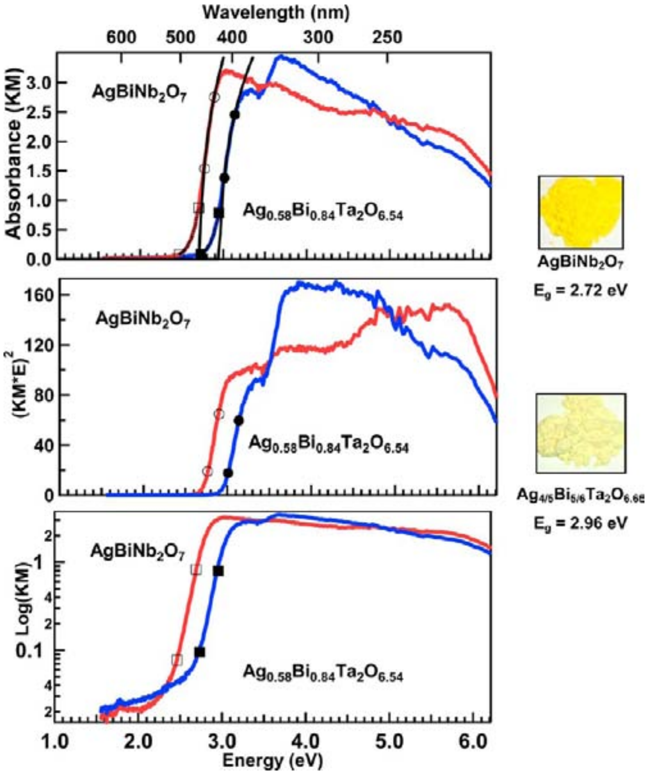

Figure 9. Room temperature UV−visible diffuse reflectance spectra of $AgBiNb_2O_7$ (red) and $Ag_{4/5}Bi_{5/6}Ta_2O_{6.65}$ (blue). Top plot shows the relative absorbance obtained from a Kubelka−Munk transform fit to a direct band gap transition (solid line, fit range marked with circles) and to an Urbach tail (dotted line, fit range marked with squares). Plots of the data that have been rescaled to give a linear response for the direct excitation model (center) and Urbach tail response (bottom) are shown.

A more quantitative understanding the optical properties of $AgBiNb_2O_7$ and $Ag_{4/5}Bi_{5/6}Ta_2O_{6.65}$ can be accomplished by analyzing the diffuse reflectance data measured for powder samples. This data has been scaled in different manners to clarify the origin of the different optical responses present in the data, as displayed in Figure 9. In all three plots the raw reflectance data has been converted via a Kubelka−Munk transform to a relative absorbance, α_{KM}, an important step since most quantitative formulas for describing the optical properties of solids describe the energy dependence of absorbance. The absorbance of both compounds drops sharply below the band gap, then slowly tails off at lower energies. The optical response below the band gap ($E < E_g$) is characteristic of an Urbach tail, whose energy dependence appears linear when the absorbance is plotted on a logarithmic scale (Figure 9, bottom) due to its functional form of $\alpha = \alpha_0 \exp[(E - E_0)/E_u]$, where α is absorption, E_u is an Urbach energy scale (which increases with increasing temperature and structural disorder), and α_0 and E_0 are constants with E_0 usually corresponding to the band gap in the case of direct band gap semiconductors. It is important to ensure that the Urbach tail does not interfere with the fitting of the main absorption edge, and we have chosen our fitting range (circles on Figure 9) to avoid this.

The energy dependence of the absorbance of semiconductors is generally described by a function which includes terms for both direct and indirect excitations: $\alpha = A/E(E - E_{g,dir})^{1/2} + B/E(E - E_{g,ind} \pm E_{ph})^2$, where $E_{g,dir}$ and $E_{g,ind}$ are the magnitude of direct and indirect gaps, respectively, E_{ph} is the emitted or absorbed phonon energy, and A and B are constants for the direct and indirect terms, respectively, with a $1/E$ dependence present in the equation to account for the typical energy variation of the refractive index of semiconductors.[21,22] More generally, the form used here for a direct gap semiconductor applies to the onset of dipole allowed absorption between two band edges and may apply to higher-lying band onsets. Similarly, the form used here for indirect gap semiconductor applies to the onset of absorption between two bands that are not dipole allowed, but which can have a second-order matrix element for absorption of light together with absorption or emission of a phonon. Finally, a semiconductor band structure may exhibit a minimum gap that is direct in *k*-space but still not have a dipole-allowed absorption associated to it. In this case, the onset in the absorption will not follow the usual 'direct gap' form, but instead the form for higher-order (e.g., quadrupole) or phonon-assisted optical transitions. The main optical response of both $AgBiNb_2O_7$ and $Ag_{4/5}Bi_{5/6}Ta_2O_{6.65}$ appears to be direct excitations (which do not involve a phonon contribution) on the basis of the quality of the fit obtained when only the direct term is used, and the clear linear scaling when the squared product of absorbance and energy ($\alpha_{KM} \times E$) is plotted vs energy.

Further insights into the nature of the valence band and conduction band levels were realized using density functional theory (DFT) electronic structure calculations. The extensive vacancies in the structure of the $Ag_{4/5}Bi_{5/6}Ta_2O_{6.65}$ pyrochlore cannot be effectively modeled by DFT methods without carrying out many calculations of possible local configurations within large supercells and then incorporating those results into computationally demanding evaluations of large representative structures obtained through Monte Carlo simulations. Our efforts were therefore restricted to niobate pyrochlores. Calculations were first focused on the relatively simple reference compound $Ca_2Nb_2O_7$, and then were broadened to consider several cation-ordered, stoichiometric models that could be used as a basis for understanding $AgBiNb_2O_7$.

Semiconductors with direct optical absorption transitions are particularly good candidates for photochemical applications since their absorption coefficient is large and light can often be completely absorbed within a thickness of 100−1000 nm.[23] The reference compound $Ca_2Nb_2O_7$ adopts a typical cubic pyrochlore structure with a = 10.4445(5) Å[24] and has a sharp onset of absorption in room temperature UV−vis diffuse reflectance data that has been previously attributed to direct excitations with an optical gap of 4.15 eV.[13] Our electronic structure calculations find $Ca_2Nb_2O_7$ to be a direct band gap semiconductor with the direct band gap occurring at the Γ point (Figure 10). The magnitude of the calculated gap is 1.40 eV, a value substantially lower than the experimental optical gap of 4.15 eV. Although this is mostly a reflection of the well-known tendency of DFT calculations to systematically underestimate the band gaps of semiconductors and insulators, another factor appears to be partially responsible for the discrepancy.

An analysis of the expected optical absorption spectrum for $Ca_2Nb_2O_7$ that only considers direct, dipole-allowed transitions based on the theoretically calculated electronic structure shows that the onset of strong absorption begins only at 1.9 eV, a substantially (0.5 eV) higher energy than the calculated band gap of 1.4 eV (Figure 10). Despite the availability of direct excitation pathways, this pyrochlore behaves analogously to indirect band gap semiconductors in that strong absorption occurs only at energies substantially higher than the actual band gap. For photoelectrochemical applications, it would therefore be expected that, at most, 3.65 eV of work could be accomplished by photons absorbed by $Ca_2Nb_2O_7$, probably not an issue for this wide band gap semiconductor since this still represents a high potential, but a possible cause for concern with regard to visible-light-absorbing analogues. The fact that the lowest direct band gap is not dipole allowed for optical absorption has been seen for other pyrochlores like $Ag_2Sb_2O_6$.[25]

The chemical origins of the electronic states that contribute to the $Ca_2Nb_2O_7$ conduction and valence bands are analyzed in the context of their density of states (DOS) in Figure 10. It can be seen that the bottom edge of the conduction band manifold is mainly composed of empty Nb 4d orbital states. The top of the valence band mainly consists of O 2p orbitals with a minor Ca 4s orbital contribution. The O1 states are located at energies of about −7 to −2 eV, while the O2 states are found between −2 to 0 eV, indicating that the O2 electronic states in the OA_4 tetrahedra are located at substantially higher energies than the O1 states in BO_6 octahedra. The fact that the states near the valence band are predominantly localized in the OA_4 tetrahedra while the low-lying conduction band states reside on the BO_6 octahedra gives an intuitive picture for why there is a lack of dipole-allowed transitions at the minimum gap, therefore making the initial optical absorption below 2.0 eV weak. The dominant role that O 2p orbitals play at the top of the valence band edge is typical of oxide semiconductors but is a key aspect of this material that we are striving to change through cation substitution. The replacement of Ca atoms with Ag and Bi atoms in $Ca_2Nb_2O_7$ pyrochlore should lead to different origins of the valence band states and will modify the pyrochlore electronic structure, since the mixing of Ag^+ (d^{10}) and Bi^{3+} (s^2) orbitals with O 2p orbitals is expected to reconstruct the states at the top of the valence band.

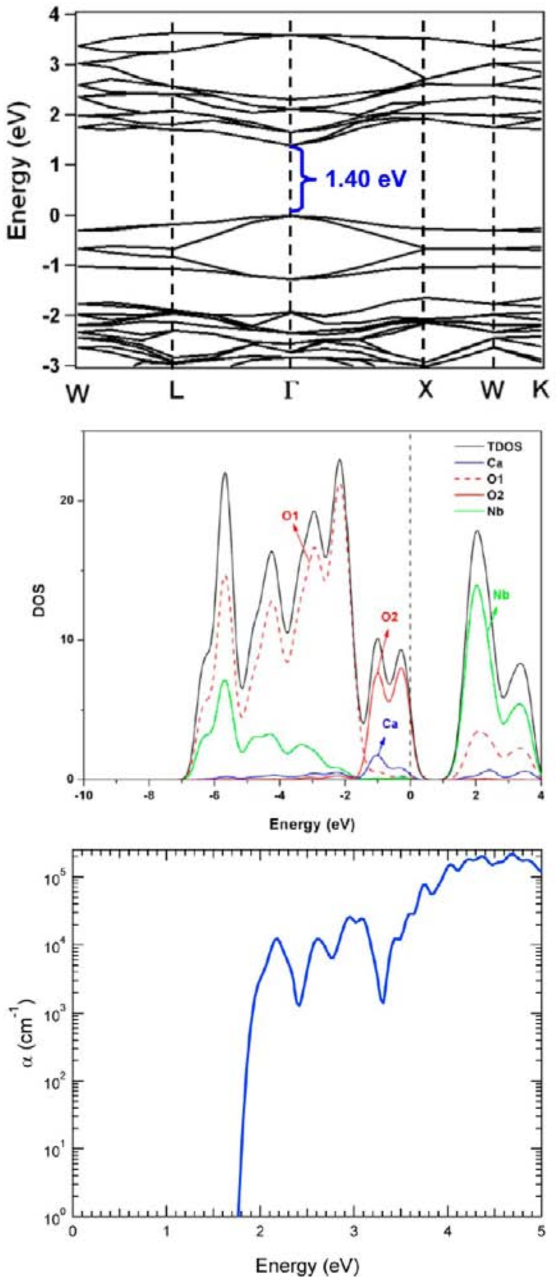

Figure 10. Band structure calculations for $Ca_2Nb_2O_7$ (with calculated band gap of 1.4 eV, top) and the density of states diagrams for $Ca_2Nb_2O_7$ with projected density of states for individual atoms (middle). Calculated absorption coefficients of $Ca_2Nb_2O_7$ (bottom).

Since the structure of $AgBiNb_2O_7$ is not yet known, three plausible models for Ag/Bi ordering were tested. In the starting cubic pyrochlore model, if just the A and O2 sites are considered, a three-dimensional corner-shared tetrahedral $[OA_4]$ network is formed. The lowest energy structures with a 1:1 Ag:Bi molar ratio are likely to involve $[OAg_2Bi_2]$

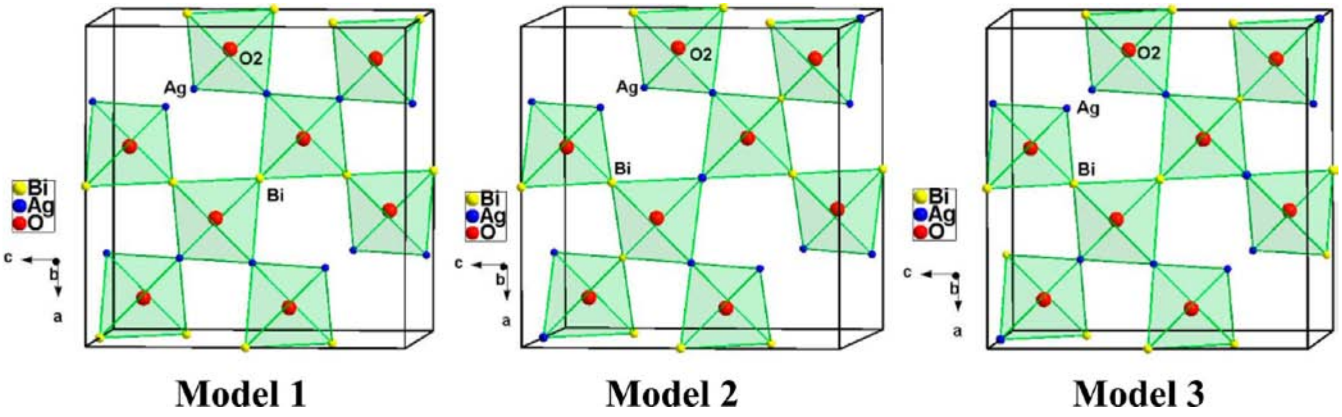

Figure 11. Three models constructed for "$AgBiNb_2O_7$" theoretical calculations by connecting $[OAg_2Bi_2]$ tetrahedra in different ways. Models 1 and 2 are centrosymmetric and model 3 is noncentrosymmetric. The Nb and O1 atoms are included in theoretical calculations but omitted here for clarity.

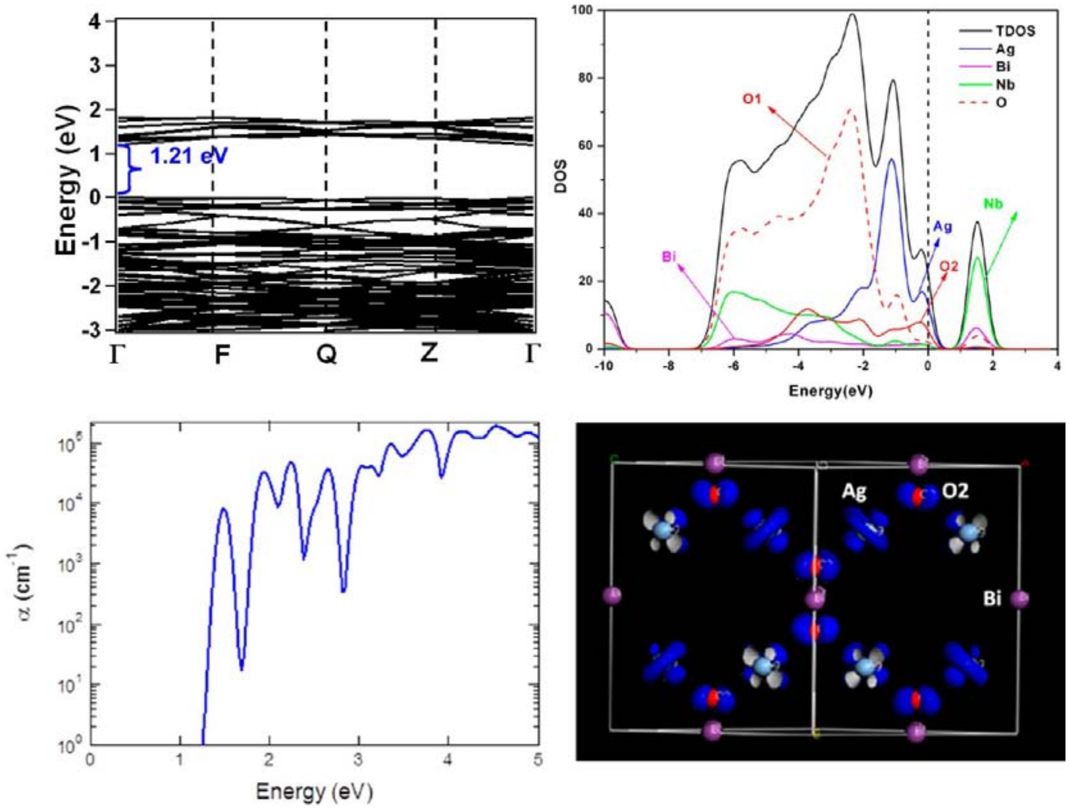

Figure 12. Band structure calculations for "$AgBiNb_2O_7$" (with calculated band gap of 1.21 eV, top left) and the density of states diagrams for "$AgBiNb_2O_7$" with projected density of states for individual atoms (top right) based on the cation-ordered structure. The strong contribution of Ag 4d (d_{z^2}) and O 2p (p_z) states to the top of the valence band can be seen in the projected electron density of these states (bottom right). The calculated $AgBiNb_2O_7$ absorbance coefficient is predicted to rapidly rise to large values (10^4–10^5 cm^{-1}) at energies not much higher than the band gap energy (bottom left).

tetrahedra with the same average charge, thereby minimizing Coulombic repulsions. A variety of cation arrangements within the base cubic pyrochlore cell can be constructed by connecting the $[OAg_2Bi_2]$ tetrahedra in different ways. Among them, only two models are centrosymmetric while the majority are noncentrosymmetric. Three models of $[OAg_2Bi_2]$ arrangements with the highest degree of symmetry (shown in Figure 11) were considered to be the most likely. DFT methods were used to relax their structures to a minimum energy configuration, and then a judgment was made about their suitability on the basis of both their total energy and the degree to which X-ray powder patterns calculated from their optimized structure matched experimental observations. Following full relaxation, model 2 and model 3 have essentially the same total energy, while model 1 is slightly higher in energy (about 0.3 eV per formula unit) higher. Of these three models, only the theoretical X-ray powder patterns generated from model 1 effectively described the observed X-ray peak diffraction positions in the experimental data. The calculated space group symmetry (*Imma*) and cell dimensions (a = 7.6333 Å, b = 7.4466 Å and c = 10.6764 Å) of this model were easily adapted to accurately fit the crystal lattice of $AgBiNb_2O_7$ in Le Bail or Pawley fits to experimental powder diffraction patterns.

Attempts to carry out Rietveld refinements of the "$AgBiNb_2O_7$" structure using the model 1 *Imma* structure were unsuccessful in accurately fitting the experimental diffraction data with reasonable structural parameters (good fits to X-ray data could only be obtained with *A*-site thermal parameter *B*-values of about 4.0, an excessively large value). However, the agreement was sufficiently close that we believe the true $AgBiNb_2O_7$ structure is closely related to the model 1 atomic arrangements, probably involving the random or systematic displacement of *A*-site cations and/or oxygens from their ideal position. We therefore use the model 1 relaxed structure as a starting point for understanding the electronic structure of $AgBiNb_2O_7$.

The results of the electronic structure and optical absorption calculations for model 1 "$AgBiNb_2O_7$" are shown in Figure 12. A direct band gap of 1.21 eV is found at the Γ point, and the calculated band gap is smaller than that of $Ca_2Nb_2O_7$ (1.41 eV). The calculated DOS (Figure 12) shows that the states at the top of the valence band are primarily composed of filled Ag $4d^{10}$ states hybridized with O 2p orbitals from the O2 site. The Bi $6s^2$ lone pair orbitals are found at a relatively accessible energy of about −10 eV, close enough in energy to the O 2p orbital manifold (dispersed from −7 to 0 eV) where the repulsive raising of O 2p states may be possible. The calculated absorption spectrum (Figure 12) exhibits an onset about 0.2 eV above the minimum direct gap. Thus, the minimum direct gap appears to be dipole forbidden in this model compound, like that in the parent compound $Ca_2Nb_2O_7$. However, the energy difference to the allowed optical transitions is much smaller—a very encouraging result for photoelectrochemical applications.

It is clear from both experiment and theory that the band gap of "$AgBiNb_2O_7$" is much smaller than that of $Ca_2Nb_2O_7$, an effect that we believe is mainly caused by the hybridization of Ag $4d^{10}$ states with the 2p orbitals of the O2 site. When the electron density at the top of the valence band is visualized, the interacting Ag d_{z^2} and O p_x orbitals can clearly be resolved (Figure 12). The decrease in the band gap is expected to come primarily from the raising of the valence band, since the character of the conduction band edge is essentially unchanged (empty Nb 4d states hybridized with O 2p orbitals from the O1 atoms, with the coordination environment of both of these species remaining constant). The low lying Bi lone pair states could also play a role in pushing up the valence band, but their influence is difficult to directly resolve in these DFT calculations. It therefore appears that combination of Ag and Bi ions is a very effective route for raising the valence band of oxide semiconductors.

In summary, optical fits indicate direct absorption of light with an optical gap of 2.96 eV for "$AgBiTa_2O_7$" and 2.72 eV for $AgBiNb_2O_7$. DFT calculations suggest that the true electronic band gap of $AgBiNb_2O_7$ is probably about 0.2 eV smaller than the optical gap. The calculations for the model, ordered structure show that the transition at the minimum direct gap is dipole forbidden. The substantial Urbach tail observed in the measured diffuse reflectance data of these compounds is believed to obscure the onset of weaker dipole-forbidden absorption expected near the minimum gap energy. The intense yellow color of "$AgBiNb_2O_7$" powders is consistent with the large values of α (10^4–10^5 cm^{-1}) obtained from first-principles calculations on the cation-ordered "$AgBiNb_2O_7$" structure (Figure 12). Taken together, these results suggest that "$AgBiNb_2O_7$" semiconductors are an excellent platform for harvesting visible light energy to drive photochemical reactions, as the band gap of this compound is similar to that of the widely utilized material WO_3 but with a much sharper onset of strong light absorption. This strong absorption suggests that thin films of "$AgBiNb_2O_7$" should be able to harvest the majority of photons with energies exceeding the band gap at micrometer or even submicrometer thicknesses.

Photoactivity testing. On the basis of their optical properties, both $AgBiNb_2O_7$ and $Ag_{4/5}Bi_{5/6}Ta_2O_{6.65}$ will be excellent candidates for driving direct water splitting if their band edge energies are appropriately positioned. The suitability of their valence band and conduction band positions can be independently tested via the use of sacrificial reagents to drive the half reactions for hydrogen production ($2\ H^+ \rightarrow H_2$) and oxygen production ($2\ H_2O \rightarrow O_2 + 4\ H^+$). While most oxide semiconductors have band edge energies suitable for driving O_2 production, it is extremely rare to find visible-light-absorbing semiconductors ($E_g < 3.0$ eV) capable of driving H_2 production in the absence of an external bias. Although measurements of both H_2 and O_2 production were attempted, only the H_2 tests were successful due to aggregation issues during tests of O_2 production.

Photochemical reactions were done with a 450 W mercury lamp. Both $AgBiNb_2O_7$ and $Ag_{4/5}Bi_{5/6}Ta_2O_{6.65}$ showed activity for hydrogen gas production in the presence of sacrificial reagent (methanol) under UV light with H_2 evolution rates are 0.86 and 1.48 μmol/h for $AgBiNb_2O_7$ and $Ag_{4/5}Bi_{5/6}Ta_2O_{6.65}$, respectively (Figure 13). The H_2 evolution rates in $AgBiNb_2O_7$ and $Ag_{4/5}Bi_{5/6}Ta_2O_{6.65}$ may be impacted by their band structure in two different manners. The valence band levels are similar for both of the compounds since they are mainly composed of hybridized Ag d^{10} and O 2p orbitals. Considering the optical direct gaps of $AgBiNb_2O_7$ and $Ag_{4/5}Bi_{5/6}Ta_2O_{6.65}$, which are 2.72 and 2.96 eV, respectively, the conduction band potential of $Ag_{4/5}Bi_{5/6}Ta_2O_{6.65}$ is expected to be more negative than that of $AgBiNb_2O_7$, providing more driving force for water reduction to form H_2 gas. An opposite trend is expected when the gap magnitudes of the two materials are considered, since $Ag_{4/5}Bi_{5/6}Ta_2O_{6.65}$ will absorb a smaller fraction of the solar spectrum due to its larger band gap.

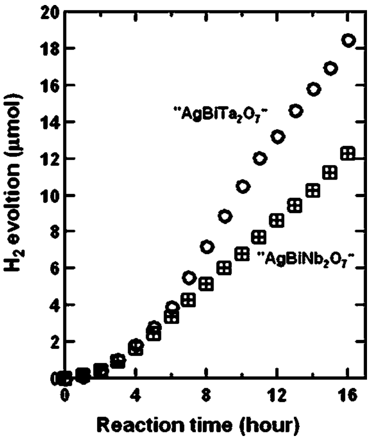

Figure 13. H_2 evolution from $AgBiNb_2O_7$ (squares) and $Ag_{4/5}Bi_{5/6}Ta_2O_{6.65}$ (circles) under UV light (λ >300 nm) irradiation (450 W high pressure Hg lamp). A 0.3 g quantity of catalyst was dispersed in 400 mL aqueous methanol solution (10 vol %) with 0.1 wt % Pt cocatalyst in situ photodeposited from H_2PtCl_6.

Although these rates of hydrogen production are low, they are very exciting since they are indicative of the successful implementation of our design strategies to raise the valence band edge of oxide semiconductors. It is likely that $AgBiNb_2O_7$ and $Ag_{4/5}Bi_{5/6}Ta_2O_{6.65}$ have suitable band edge positions for driving overall water splitting with visible light, given the deep valence band positions routinely observed for oxides. However, O_2 gas evolution could not be effectively tested in this system since the powder particles were observed to aggregate together around the stir bar when illuminated and could not be effectively dispersed in an $AgNO_3$ test solution. Furthermore, attempts to more quantitatively measure band edge positions through Mott−Schottky analysis of capacitance data were unsuccessful due to the challenges of preparing suitable electrodes with the large particles sizes (>1 μm) of synthesis products.

Given the promising nature of the band alignment and the effective light absorption of this system, it is important to ask why the H_2 evolution rate is low and if there are routes by which this can be overcome. We attribute the major activity limitation to the large particle size observed in SEM measurements of these ceramics (Figure 14) that is related to the low melting points of both Ag and Bi. It can be seen from the images that both $AgBiNb_2O_7$ and $Ag_{4/5}Bi_{5/6}Ta_2O_{6.65}$ have large (1−10 μm) and well-faceted primary particles that form even larger secondary particles due to either partial melting of an intermediate phase or through a very effective sintering process enabled by low melting point constituents. These particle sizes far exceed the expected minority carrier diffusion lengths of complex oxide semiconductors (10−100 nm), and it is expected that most photogenerated carriers within these large particles cannot even diffuse to the surfaces before recombination occurs. Initial attempts to synthesized nanoscale powders were unsuccessful due to the challenges of simultaneously dissolving the disparate chemical constituents. A more promising route that we are pursuing further is the preparation of thin films using physical vapor-deposition techniques.

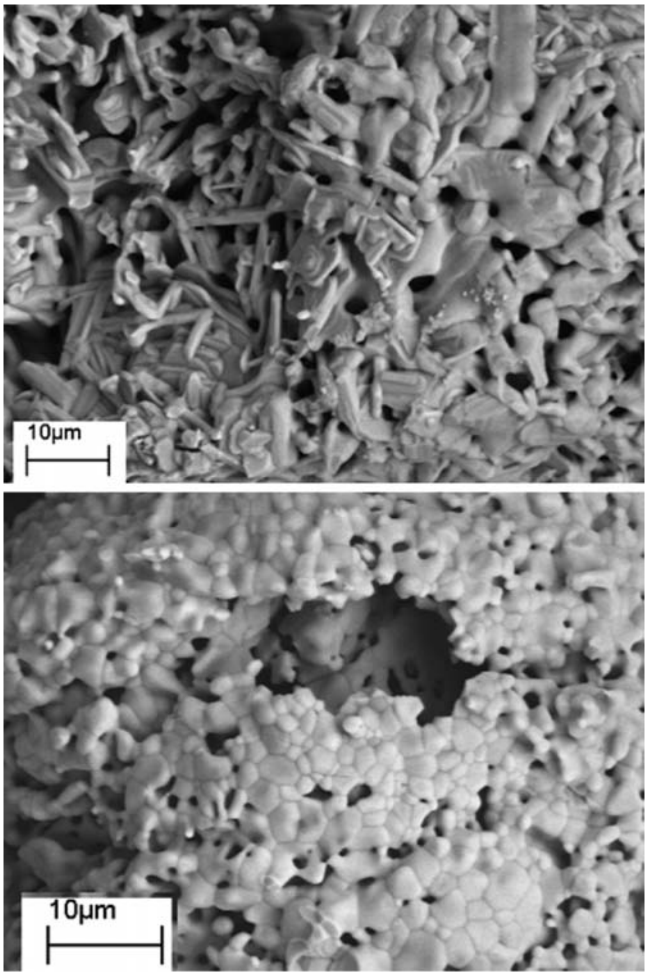

Figure 14. SEM images of $AgBiNb_2O_7$ (top) and $Ag_{4/5}Bi_{5/6}Ta_2O_{6.65}$ (bottom) heated at 1000 °C.

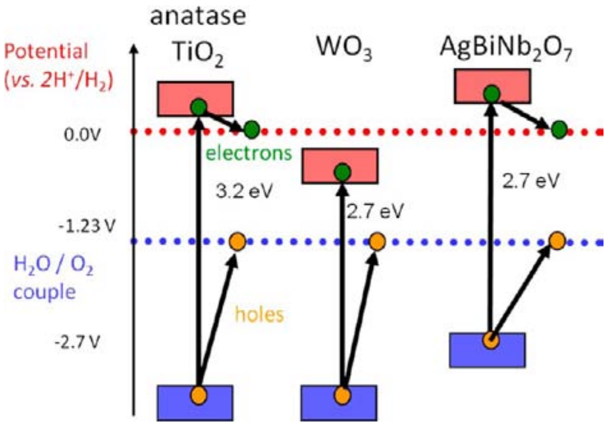

Figure 15. Schematic comparison of the conduction band and valence band edge positions in UV-absorbing anatase TiO_2 and in visible-light-absorbing WO_3 and $AgBiNb_2O_7$. The compound $AgBiNb_2O_7$ appears more suitable for visible light harvesting for water splitting than WO_3 due to its raised band edge energies and its intense direct band gap absorption, and is a rare example of a visible-light-absorbing oxide with energy levels suitable for driving both O_2 and H_2 production.

The improvements in the electronic states of $AgBiNb_2O_7$ relative to the canonical oxide semiconductors TiO_2 and WO_3 are schematically illustrated in Figure 15. Most oxide semiconductors with conduction band edge energies suitable for driving H_2 production are wide band gap semiconductors like anatase TiO_2 (E_g = 3.2 eV). Most visible-light-absorbing semiconductors like WO_3 (E_g = 2.7 eV) cannot drive H_2 production since their reduced band gap (relative to UV-absorbers) is mainly due to lowering of the conduction band position to an extent that the H_2 production is shut off, rather than an increase in the valence band edge position, which in oxide semiconductors is typically found about 3.0 eV below the 2 H^+/H_2 redox couple. Although the optical gap of $AgBiNb_2O_7$ is comparable to that of WO_3, its valence and conduction band energies are substantially raised relative to those of WO_3, permitting $AgBiNb_2O_7$ to drive H_2 production with visible light. The strong optical absorption at energies slightly higher than the band gap (calculated α of 10^4−10^5 cm^{-1}) indicate that this compound can potentially serve as a far better platform for light harvesting than the indirect band gap semiconductor WO_3. It is therefore of great importance to further develop synthetic routes for this oxide semiconductor that will allow it to be produced with nanoscale dimensions that should enable it to efficiently drive photochemical processes.

CONCLUSIONS

Two complex oxide semiconductors materials were designed and synthesized as candidates for visible-light-driven water splitting. One compound adopts the pyrochlore structure with a stoichiometry refined from neutron and X-ray diffraction data as $Ag_{4/5}Bi_{5/6}Ta_2O_{6.65}$. The second compound was found to have an integer stoichiometry of "$AgBiNb_2O_7$" and has an orthorhombic structure that is suggested to arise from Ag/Bi cation ordering based on DFT calculations and the indexing of powder diffraction data. Both compounds are yellow in color, indicative of their capability to absorb visible light, with an optical direct gap determined from UV−vis spectra to be 2.72 eV for Nb and 2.96 eV for Ta. Theoretical calculations showed that the hybridized Ag 4d and O 2p orbitals play an important role in narrowing the band gap by raising the energy of the valence band. These calculations confirm the strong onset of absorption in $AgBiNb_2O_7$ at an energy that is slightly above the minimum band gap (about 0.2 eV) involving transitions between slightly higher-lying energy bands. Photocatalytic activity measurements showed that both compounds can produce H_2 gas under UV light illumination in the presence of sacrificial reagents. This suggests that their valence band edge is substantially raised relative to typical oxides, and overcomes a major barrier to realizing efficient visible-light-driven water splitting oxide semiconductors. Although large particle sizes have thus far precluded an effective test of overall water splitting using these semiconductor systems, these compounds have very promising light-harvesting capabilities for direct water splitting applications with visible light.

ASSOCIATED CONTENT

Ⓢ Supporting Information

Two TOPAS input files (as TXT files) used for Rietveld refinement, and the two CIF files with the results of the $Ag_{4/5}Bi_{5/6}Ta_2O_{6.65}$ structural refinement in both the displacive and nondisplacive models. Spectrum of light used for photactivity measurements. This material is available free of charge via the Internet at http://pubs.acs.org.

AUTHOR INFORMATION

Corresponding Author

*Tel.: (631)632-7996. E-mail: kpete@bnl.gov.

Present Addresses

¶General Electric (China). Tel.: +86-21-38771985. E-mail: Limin.Wang@ge.com.

#Peking University, Center for Applied Physics and Technology. Tel.: +86-10-62754177. E-mail: weikang@pku.edu.cn.

○Department of Chemistry, Tokyo Institute of Technology. Tel.: +81-3-5734-2239. E-mail: maedak@chem.titech.ac.jp.

Notes

The authors declare no competing financial interest.

ACKNOWLEDGMENTS

This work was in part carried out at BNL under Contract DE-AC02-98CH10886 with the U.S. Department of Energy. We also gratefully acknowledge the U.S. DOE for funding under the BES Hydrogen Fuel Initiative. The portion of this Research at Oak Ridge National Laboratory's Spallation Neutron Source was sponsored by the Scientific User Facilities Division, Office of Basic Energy Sciences, U.S. Department of Energy. Use of the National Synchrotron Light Source, Brookhaven National Laboratory, was supported by the U.S. Department of Energy, Office of Science, Office of Basic Energy Sciences, under Contract No. DE-AC02-98CH10886. Diffuse reflectance experiments and DFT computations were done at Brookhaven National Laboratory's Center for Functional Nanomaterials (CFN), which is supported by the Department of Energy under grant DE-AC02-98CH10886. We are very appreciative of the efforts of Dr. James Ciston (LBNL) to investigate the structure of these materials through electron diffraction at the BNL CFN, despite the complications induced by beam damage. Many thanks go to Prof. Peter Stephens and Saul Lapidus for enabling the collection of high-resolution powder diffraction data which helped enable the indexing of this data, as well as for extensive informal tutorials on advanced powder diffraction methods.

REFERENCES

(1) Kudo, A.; Miseki, Y. *Chem. Soc. Rev.* **2009**, *38*, 253−278.
(2) Osterloh, F. E. *Chem. Mater.* **2008**, *20*, 35−54.
(3) Maeda, K.; Domen, K. *J. Phys.Chem. Lett.* **2010**, *1*, 2655−2661.
(4) Kudo, A.; Miseki, Y. *Chem. Soc. Rev.* **2009**, *38*, 253−278.
(5) Maeda, K.; Domen, K. *J. Phys. Chem. C* **2007**, *111*, 7851−7861.
(6) Larson, A. C.; Dreele, R. B. V. *Los Alamos National Laboratory Report LAUR* **2000**, 86−748.
(7) Toby, B. H. *J. Appl. Crystallogr.* **2001**, *34*, 210−213.
(8) Clark, S. J.; Segall, M. D.; Pickard, C. J.; Hasnip, P. J.; Probert, M. J.; Refson, K.; Payne, M. C. *Z. Kristallogr.* **2005**, *220*, 567−570.
(9) Vanderbilt, D. *Phys. Rev. B* **1990**, *41*, 7892−7895.
(10) Perdew, J. P.; Burke, K.; Ernzerhof, M. *Phys. Rev. Lett.* **1996**, *77*, 3865−3868.
(11) Takahashia, H.; Kakihanab, M.; Yamashitab, Y.; Yoshidab, K.; Ikedac, S.; Hara, M.; Domen, K. *J. Alloys Compd.* **1999**, *285*, 77−81.
(12) Ikeda, S.; Fubuki, M.; Takahara, Y. K.; Matsumura, M. *Appl. Catal., A* **2006**, *300*, 186−190.
(13) Wu, J.; Li, J.; Lue, X.; Zhang, L.; Yao, J.; Zhang, F.; Huang, F.; Xu, F. *J. Mater. Chem.* **2010**, *20*, 1942−1946.
(14) Grey, I. E.; Roth, R. S.; Mumme, W. G.; Planes, J.; Bendersky, L.; Li, C.; Chenavas, J. *J. Solid State Chem.* **2001**, *161*, 274−287.
(15) Levin, I.; Amos, T. G.; Nino, J. C.; Vanderah, T. A.; Randall, C. A.; Lanaganw, M. T. *J. Solid State Chem.* **2002**, *168*, 69−75.
(16) Melot, B.; Rodriguez, E.; Proffen, T.; Hayward, M. A.; Seshadri, R. *Mater. Res. Bull.* **2006**, *41*, 961−966.
(17) Krayzman, V.; Levin, I.; Woicik, J. C. *Chem. Mater.* **2007**, *19*, 932−936.
(18) Nguyen, H. B.; Noren, L.; Liu, Y.; Withers, R. L.; Wei, X.; Elcombe, M. M. *J. Solid State Chem.* **2007**, *180*, 2558−2565.
(19) Liu, Y.; Withers, R. L.; Nguyen, H. B.; Elliott, K.; Ren, Q.; Chen, Z. *J. Solid State Chem.* **2009**, *182*, 2748−2755.
(20) Brese, N. E.; O'Keeffe, M. *Acta Crystallogr., Sect. B* **1991**, *47*, 192−197.
(21) Pankove, J. I. *Optical Processes in Semiconductors*; Dover Publications: New York, 1971.
(22) Singh, D. J.; Rai, R. C.; Musfeldt, J. L.; Auluck, S.; Singh, N.; Khalifah, P.; McClure, S.; Mandrus, D. G. *Chem. Mater.* **2006**, *18*, 2696−2700.
(23) Walter, M. G.; Warren, E. L.; McKone, J. R.; Boettcher, S. W.; Mi, Q.; Santori, E. A.; Lewis, N. S. *Chem. Rev.* **2010**, *110*, 6446−6473.
(24) Lewandowski, J. T.; Pickering, I. J.; Jacobson, A. J. *Mater. Res. Bull.* **1992**, *27*, 981−988.
(25) Allen, J. P.; Nilsson, M. K.; Scanlon, D. O.; Watson, G. W. *Phys. Rev. B* **2011**, *83*, 035207.